Autonomous Landing of an UAV with a Ground-Based Actuated Infrared Stereo Vision System

Weiwei Kong, Daibing Zhang, Xun Wang, Zhiwen Xian and Jianwei Zhang

***Abstract*— In this study, we focus on how to land an unmanned aerial vehicle (UAV) in unknown and GPS-denied environments based on an infrared stereo vision system. The vision system is fixed on the ground and used to track the UAV's position during the landing process. In order to enlarge the search field of view (FOV), a pan-tilt unit (PTU) is employed to actuate the vision system. The infrared camera is chosen as the exteroceptive sensor for two main reasons: first, it can be used round the clock under all-weather conditions; second, infrared target can be tracked based on infrared spectrum features at a lower computational cost compared to tracking texture features. State-of-the-art active-contour based algorithms and the meanshift algorithm have been evaluated with regard to detecting and tracking an infrared target. Field experiments have been carried out using a Microdrone unmanned quadrotor and a fixed-wing unmanned aircraft, with both qualitative and quantitative evaluations. The results demonstrate that our system can track UAVs without artificial markers and is sufficient to complement for or replace the GPS-based localization in GPS-denied environment or where its information is inaccurate.**

I. INTRODUCTION

In the past decades, unmanned aircraft systems (UASs) have emerged in an increasing number of applications, mostly for military but also civilian. Nowadays, safe autonomous flight during the whole assignment is essential for wide spread acceptance of aircraft, where safely landing is the last but not least crucial maneuver. Autonomous landing an unmanned aerial vehicle (UAV) in unknown, GPS-denied environments is still an open problem. The key challenges here are to robustly control an unstable UAS and to localize the UAS only using information from vision sensors even under potential sensor loss.

The goal of this research is to provide UAV with an additional vision-based source of information, extracted by ground cameras. We provide an affirmative answer to the question of whether on-ground stereo vision systems can be used to sustain real-world GPS-denied flight, by presenting an actuated infrared stereo vision system that is validated through autonomous flight-tests. The main idea is to track the UAV during the landing process and estimate the relative position between the UAV and its landing point, based on the above mentioned vision system. The system, as the primary senor for tracking and landing, has been evaluated by field experiments. Our landing system is constructed by an infrared stereo and a PTU, which is shown in Fig. 1. One of the great interests to the control community is vehicle navigation. According a recent survey [1], with regard to UAV, navigation can be defined as the process of data acquisition, data analysis, as well as extraction and inference of information about the vehicle's states and its surrounding environment, with the objective to accomplish assigned missions successfully and safely. There are four core functions in a navigation system, from lower to higher level, being Sensing, State Estimation, Perception, and Situational Awareness. Regarding to the four functions, different types of sensors such as the Global Navigation Satellite System (GNSS), laser range scanners (LRFs)[2][3], monocular cameras[4][5], stereo cameras and the newly populated RGB-D sensors[6][7] have been explored. With respect to solving the landing problem, most previous researches rely on on-board sensors[8][4] where experiments have been conducted in both indoor- and outdoor- environments. Ground systems on the other hand[9][10][11], have not been so widely considered for autonomous landing, in particular with infrared stereo vision. Furthermore, the Sierra Nevada Corporation has developed the Tactical Automated Landing System(TALS) based on millimeter wavelength ground radar for autonomous landing [12], which is an all-weather ground station. However, there are some disadvantages in aforementioned autonomous landing systems: (1) Since the payload of UAV is limited, this makes a strong restriction for sensor selection considering their weights. (2) For most of the field UAVs, the position and velocity estimation are based on GPS. However, in some circumstances, such as

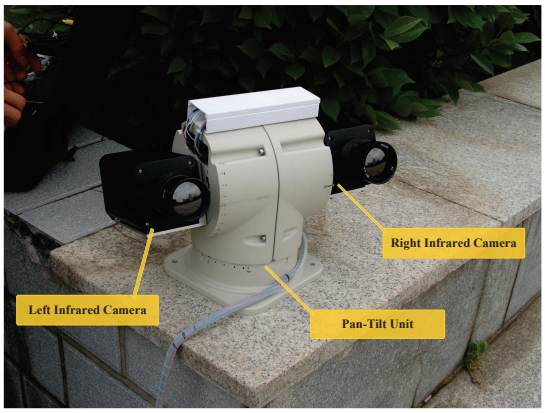

Fig. 1. Infrared stereo system with PTU.

Weiwei Kong, Daibing Zhang, Xun Wang and Zhiwen Xian are with College of Mechatronic Engineering and Automation, National University of Defense Technology (NUDT), Changsha 410073, China. (Corresponding author: Weiwei Kong, e-mail: kong@informatik.uni-hambrg.de).

Jianwei Zhang is with the Institute of Technical Aspects of Multimodal systems(TAMS), Department of Computer Science, University of Hamburg, Germany

urban or low altitude operations, GPS receiver antenna is prone to losing line-of-slight with satellites and GPS cannot consequent support high quality position information [13], which is quite dangerous for closed-loop control system in the landing maneuver. (3) Recent ground vision systems either are based on artificial markers [14][15] or have limited range of observation[11].

Therefore, above mentioned considerations rule out employing such position sensors as GPS and places emphasis on other passive sensors. Besides, we do not employ radar (such as TALS), LRFs or other active range sensors, because we deliberately refrain from using expensive, customized hardware and the desire to avoid detection. In order to deal with these problems, we have built an infrared vision based ground landing system whose FOV is enlarged by a PTU, providing an alternative to exist systems.

The contributions of this work are three-fold:

- First, a custom-built perception platform with a large FOV and can be employed round the clock under all-weather conditions.
- Second, several state-of-the-art image processing algorithms have been evaluated and benchmarked against each other according to infrared targets detection and tracking.
- Third, the whole system has been tested using field experiments, with a quadrotor and a fixed-wing aircraft.

The remainder of the paper is organized as follows: In the next section, we give a short overview of related works. Then in Section III, we describe the hardware and software of our landing system. The stereo infrared calibration method, target tracking algorithms and pose estimation for the aircraft is described in Section IV, followed the experimental results in Section V.

II. RELATED RESEARCH

In this section, we discuss some previous works related to autonomous vision based landing. In last decade, vision based pose estimation has been extensively studied, such as in [16], [17] and [18]. As discussed in [1], except conventional IMU/GPS systems and state estimation using range sensors, vision-based state estimation systems can be classified into six main categories: *On-ground Vision* (OGV), *Visual Odometry* (VO), *Target Relative Navigation* (TGRN), *Terrain/landmark relative navigation* (TGR), *Concurrent Estimation of Motion and Structure* (SFM and SLAM) and *Bio-inspired Optic Flow Navigation* (BIOFN). Among the above methodologies, TGRN is one of the important assignments of vision based autonomous control. A potential application of it is autonomous, precise and safe landing.

An early autonomous navigation system for a model-scale helicopter (the Hummingbird) was reported in [19]. This system solely depended on GPS, which was traditionally favored as the primary navigation sensor. Furthermore, a number of significant achievements for UAV have been obtained based on fusing GPS and IMU [8][20][21]. However, there are many situations where GPS is not reliable, because the GPS signal can be lost due to multipath, satellites being occluded by building or even international jamming. To deal with these problems, vision based UAV control systems have been proposed. In [22], a vision-augmented navigation system for autonomous helicopter was presented where vision information is employed in the control loop. [23] proposed the visual odometer, which is a significant milestone for vision-based technique, able to provide accurate position and velocity. While various researches have tested the visible light camera based system both indoor [24][25] and outdoor [26][27][28], their common drawback is that the computational complexity is too high under cluttered environments. In addition, since UAV is expected to be operated round the clock under all-weather conditions, IR camera is clearly a proper choice. Yakimenko[29] constituted an on-board infrared vision system for UAV shipboard landing, where IR has been found capable to simplify the relative pose estimation problem and reduce the susceptibility to glare. In [30], a micro infrared camera has been used to detect infrared spots on the ground to estimate the relative position. Such infrared systems however rely on artificial makers, hence not suited for general UAV application. IR is also employed in our system but in a different manner, in order to eliminate the requirement of artificial markers.

One pivotal choice for vision systems is the number of cameras. Monocular camera has been utilized as a feedback sensor in [31][16]. [32][33] used a downward-looking camera to detect the landing pad and search safe site in hazardous terrain. [34] presented a camera fixed on the front of an UAV to detect lines of the target runway. Unlike for binocular stereo vision, these algorithms have to not only detect significant features but also compute the motion between images which increases the burden of the on-board computer. In addition, stabilizing controllers based on monocular camera [35] are subject to drift over time. To eliminate the drift, Engel[36] presented an efficiency algorithm in which the camera is fused with other sensors such as GPS, IMU and pressure altimeter. However, there is an evident increase in system complexity. Stereo vision systems have also been employed in some early work [26][27][37], due to the fact that a stereo system can estimate depth information in a single frame, and stereo could also be used to aid in outlier rejection for structure-from-motion algorithms. Then, another kind of camera set-up was presented in [15], namely trincoular. This kind of system is composed by three or more cameras for extracting key features in order to obtain robust 3D position estimation. Further, another approach close to ours is [11], which presented a system using an step motor controlled web camera to recognize markers patched on the micro-aircraft. However, the weakness of this ground system is that the FOV is narrow. A more complicated system was shown in [37] which contain two ground-based cameras and an on-board camera looking downwards.

Considering the dangerous nature of the UAV landing maneuver, system complexity is a reasonable price to pay for more robustness, so we presented a calibrated binocular infrared landing system to estimate relative position between UAV and landing site.

(a) (b)

Fig. 2. (a) md4-200 quadrotor platform (b) fixed-wing platform

TABLE I
THE TECHNICAL SPECIFICATIONS OF MD4-200

Items	Description
Vehicle mass	800g
Maximum Payload mass	300g
Diameter	540mm from rotor shaft to rotor shaft
Flight duration	up to 30 minutes
Cruising speed	8.0m/s
Climb rate	7.0m/s

III. SYSTEM ARCHITECTURE

A. Our Experimental platform

Two kinds of UAV platforms have been employed to evaluate the vision system, namely a quadrotor and a fix-wing vehicle. The quadrotor platform is an commercial product from microdrones GmbH, with the type md4-200. This platform can fly by remote control or autonomously with the aid of our GPS waypoint navigation system. Additionally, the infrared features of four brushless motors are distinct compare to the background. The specification of md4-200 platform is detailed in Table I, and Fig. 2(a).

The fixed-wing platform was selected with considerations of stable flight performance and landing in proper speed. Because the UAV is detected by infrared sensor, a propeller should not be at the end of the body, so a puller-type medium size airplane was preferred as shown in Fig. 2(b), named Stormy Petrel. The length of Stormy Petrel is 1295 mm with 1575 mm wingspan and 5.7 kg weight. The maximum speed is 120 km/h and the cruising speed is 90 km/h, equipped with ZENOAH G260PU-EI 26 CC motor.

Now we introduce the navigation module and autopilot module. iFLY-G2 (G2) is a small six-DOF (degree of freedom) navigation system, providing two combined navigation modes, i.e., GPS/INS and Attitude and Heading Reference System with Dead Reckoning(AHRS/DR). G2 includes a triaxial gyro, triaxial accelerometer, triaxial magnetic field meter, GPS module, barometric altimeter, airspeed gauge and thermometer. It provides real-time 3D information including attitude angle, angular rate, position, speed, acceleration, true air speed, calibrated air speed. The autopilot system is iFLY-F1A. It consists of the F1A autopilot system, a ground control station, a redundant power management module and an engine RPM monitoring module. iFLY-F1A is connected with iFLY-G2 through RS232, they are depicted in Fig. 3(a) and Fig. 3(b).

(a) (b)

Fig. 3. (a) iFLY-G2 Module (b) iFLY-F1A Module

B. Stereo Vision System

The stereo vision system is built on two infrared cameras, with model IRT301, which are produced by IRay Technology Co., Ltd. This kind of camera is an online surveillance infrared thermal imager. The detector materials is cooled MCT (HgCdTe) FPA and the sensor patch is 30 μm$\times$30 μm. The pixel resolution of the camera video is 320$\times$256 at 50 FPS. The focal length of the camera lens installed in the system is 22 mm with a Wide Field of View (WFOV) 24.6$\times$19.8 (in deg) , Medium Field Of View (MFOV) 4 $\times$3.2 and Narrow Field of View (NFOV) 0.92$\times$0.73. The spectral range is 3.7 μm$\times$4.8 μm. Generally, a man (1.8m$\times$0.5m) can be detected at the range 12km and recognized at 6km, which is sufficient for the landing process. The PTU to actuate the stereo vision systems is PTS-3060 from PTS General Electronics Co., Ltd. PTS-3060 features internal wiring with slip-ring for 360-continuous pan with a tilt range from -30 to +90 deg. The range of pan speed is from 0.9 to 60 deg/second and the range of tilt range is from 0.9 to 40 deg/second. The assembled stereo vision system is illustrated in Fig. 1.

C. Communication System

The communication between the UAV and ground station is based on XTend RF Modems. This modem is a 900 MHz/1W device with up to 22km outdoor RF line-of-sight range. The interface data rate is form 10 bps to 230,000 bps. Under differential GPS (DGPS) navigation system, the DGPS information is transferred to UAV. Otherwise, the vision information is transferred. The spatial information is changed to 3D relative position estimated by the ground system. The complete experimental setup is shown in Fig. 4 and the overall architecture of the system is shown in Fig. 5.

IV. CALIBRATION AND TRACKING

In this section, we introduce the methods used for system calibration and target tracking with infrared characteristics.

A. Infrared Camera Calibration

Camera calibration is the process of estimating the *Intrinsic Parameters* and *Extrinsic Parameters* of a stereo camera system. Generally, focal length, skew, distortion and image center are described by the camera's internal characteristics. On the other hand, extrinsic parameters deal with its position and orien tation in the world. Infrared stereo camera calibration is similar to that of the visible

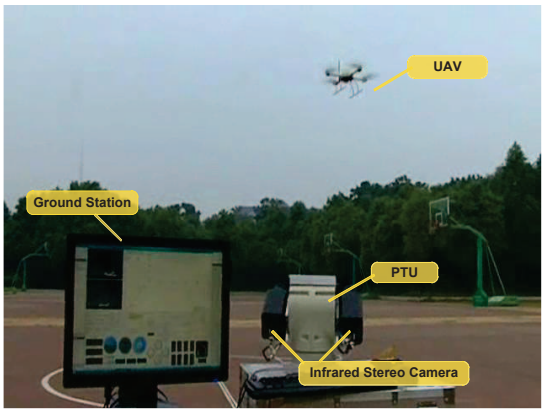

Fig. 4. Ground stereo vision landing system.

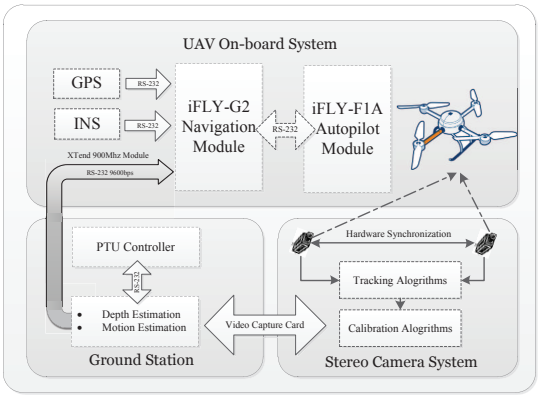

Fig. 5. Architecture of the system.

camera because of the mechanical structure. In addition, for 3D computer vision, knowing intrinsic parameters is an essential step. To achieve the intrinsic parameters, chessboard pattern is recommended since it appears to produce accurate results. However, chessboard printed on the general paper cannot be distinctly captured by infrared sensors due to no apparent temperature difference between black squares and white squares. Without clearly intersection or corner features, calibration accuracy will decrease or even failed.

Thus, by pasting the black squares on the mirror, the new pattern was designed and heated by a heater before implementing calibration algorithm (see Fig.6(a)). Then, the pattern with infrared feature can be obviously imaged by the infrared camera. One of the calibration image is shown in Fig.6(b). With respect to long distance calibration, a 3 m×3 m wood frame pattern was constructe. Each point of intersection was a heated incandescent lamp aim at enhancing the infrared features. The outcome of wood frame pattern in 50 m distance is shown in Fig.7.

B. Target Tracking Alogrithms

In this section, we briefly review some of previous work on snakes or active contours based on ideas from curvature driven flows and the calculus of variations. Tracking is one of the basic control problems, in which we want to the output to track or follow a standard signal and more importantly we

(a)

(b)

Fig. 6. (a) Black squares pasted on mirror and heated by heater. (b) Infrared features of the heated claibration board.

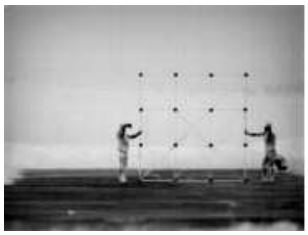

Fig. 7. Architecture of the system.

attempt to make the tracking error as small as possible. In addition, the problem of visual tracking differs from standard tracking problem in the situation that the feedback signal is measured by imaging sensors. The information from imaging sensors has to be extracted via computer vision algorithms and interpreted by specific scheme before being calculated in the control loop. The complexity in this problem comes from the fact that there is no prior information of the relative position between UAV and ground system. Inevitably, the landing system must successfully identify and track UAV and support high accuracy relative position in a short period. Both of the above methods work well in certain circumstance, but this paper. Reliable evaluation of attitude, especially the height, will increase the safety of operation of unmanned aerial vehicle during the landing process.

1) Meanshift Method[38]: Meanshift method is one of the simple and fast visual tracking algorithms. This algorithm creates a confident map in the new frame maily based on color histogram of the object in the previous image. The basic Meanshift tracking algorithm is consist of five basic steps. Given q_u of model and locaton $\mathbf{y}$ of target in previous fame: (1) Initialze locatin of target in current frame as $\mathbf{y}$. (2) Compuate $p_u(\mathbf{y})$, $u = 1, \ldots, m$ and $\rho_u(\mathbf{y}, q)$. (3) Compute weight $w_i, i = 1, \ldots, n_h$. (4) Apply Meanshift: Compute new location $\mathbf{z}$ as

$$\mathbf{z} = \frac{\sum_{i=1}^{n_h} w_i g(\left\| \frac{\mathbf{y}-\mathbf{y}_i}{h} \right\|^2)\mathbf{y}_i}{\sum_{i=1}^{n_h} w_i g(\left\| \frac{\mathbf{y}-\mathbf{y}_i}{h} \right\|^2)} \tag{1}$$

where $g(x) = -k'(x)$ and $k(x) = \frac{1}{\sqrt{(2\pi)^d}} exp(-1/2 \left\|\mathbf{x}\right\|^2)$ (5) Compute $p_u(\mathbf{y}), u = 1, \ldots, m$, and $\rho_u(\mathbf{y}, q)$. (6) While $\rho_u(\mathbf{y}, q) < \rho_u(\mathbf{z}, q)$, do $\mathbf{z} \leftarrow \frac{1}{2}(\mathbf{y} + \mathbf{z})$. (7) if $|\mathbf{z} - \mathbf{y}|$ is small engouth, stop. Else, set $\mathbf{y} \leftarrow \mathbf{z}$ and goto Step 1.

2) Snakes, Level Set Method and Fast Marching Method: Some previous works, in [39][40], demonstrated that active

contours is an autonomous processes which employ image coherence in order to track various features of interest over time. A book [41] and the references therein described snakes fit very spontaneously into a control framework. Additionally, they have been utilized in conjunction with Kalaman filtering. The kernel idea of the snakes is viewpoint of energy. During the evolution of the contour, the splines are governed by an energy functional which defines the image dependent forces, internal forces, and certain constraints set by the user. The geometric active contour or snakes method is used to identify contours. The active contour method is an iterative method in which the calculus of variations is used to control the movement of a curve within the image. The starting point of Level Set Method is [42][43] in which an active contour model founded on the level set formulation of the Euclidean curve shortening equation is proposed. Specifically, the model is:

$$\frac{\partial \Psi}{\partial t} = \phi(x,y) \left\| \nabla \Psi \right\| (\mathtt{div}(\frac{\nabla \Psi}{\left\| \nabla \Psi \right\|}) + \nu) \qquad (2)$$

Here the function $\phi(x,y)$ depends on the given image and is used as a "stopping term". Generally the term $\phi(x,y)$ is selected to be small near an intensity-based edge and acts to stop evolution when the contour gets close to an edge. According to [42][43], one may define $\phi(x,y) = \frac{1}{1+\|\nabla G_\sigma * I\|^2}$ where I is the grey-scale intensity of pixel x, y and G_σ is a Gaussian smoothing filter. The function $\Psi(x,y,t)$ evolves in equation (2) according to the associated level set flow for planar curve evolution in the normal direction with speed as a function of curvature which was discussed in [44][45].

On the other hand, the idea of length/area minimizing will modify the model in a precise manner. A curve could be explained as a one parameter p , $C = (x(p), y(p))^T$, and we change the arc-length function as, $ds = (x_p^2 + x_p^2)^{1/2}$ to $ds_\phi = (x_p^2 + x_p^2)^{1/2}\phi dp$ where $\phi(x,y)$ is appositive differentiable function. Then the new metric ds_ϕ is relative to corresponding gradient flow for shortening length.

The length function L_ϕ is defined as $L_\phi = \int_0^1 \left\| \frac{\partial C}{\partial t} \right\| \phi dp$. Then, by taking the first variation of the modified length function L_ϕ and using integration by parts as in, we get that

$$L'_\phi(t) = -\int_0^{L_\phi(t)} \left\langle \frac{\partial C}{\partial t}, \phi \kappa \vec{N} - (\nabla \phi \cdot \vec{N}) \vec{N} \right\rangle \qquad (3)$$

where $\kappa = \|C_{ss}\|$ is the curvature, and $\vec{N} = \frac{1}{\kappa} C_{ss}$ denotes the unit normal to the curvature C. The level set version of this is $\frac{\partial \Psi}{\partial t} = \phi \left\| \nabla \Psi \right\| \mathtt{div}(\frac{\nabla \Psi}{\left\| \nabla \Psi \right\|}) + \nabla \phi \cdot \nabla \Psi$. This evolution should attract the contour very quickly to the feature which lies at the bottom of the potential well described by the gradient flow. As in [44][45], in order to keep shrinking the contour, we may also add a constant inflation term, and so derive a modified model of (2) given by

$$\frac{\partial \Psi}{\partial t} = \phi \left\| \nabla \Psi \right\| \mathtt{div}(\frac{\nabla \Psi}{\left\| \nabla \Psi \right\|} + \nu) + \nabla \phi \cdot \nabla \Psi \qquad (4)$$

Then, a well-known *Eikonal equation* $\phi(x,y) \left\| T(x,y) \right\| = 1$ is built based on crossing time. Fast Marching Method can solve this Eikonal Equation through difference operator.

TABLE II
THE SUCCESSFUL DETECTION PERCENTAGE OF FIVE DIFFERENT METHODS

Scene	Frames	Meanshift	Snakes	LSM	DRLSE	FMM
1	389	87.4	97.7	98.2	100.0	100.0
2	1143	72.19	99.7	99.9	100.0	100.0
3	359	94.7	97.5	97.5	100.0	100.0
4	892	0.0	98.7	98.7	100.0	100.0
5	80	92.5	97.5	100.0	100.0	100.0

[46] tested the Fast Marching Method to estimate the relative location between two UAVs.

3) Distance Regularized Level Set Evolution(DRLSE)[47]: This method is a new type of level set evolution in which regularity of the level set function is intrinsically maintained. Besides, using the relatively large time steps, iteration numbers and computattion time of DRLSE are reduced, while ensures acccurate computation and stabel level set evolution.

V. EXPERIMENTS

We have conducted a series of field experiments to evaluate the stereo vision system. The experiments were carried out in different environments during both day and night. In the following, tracking experiments are detailed in Section V-A. Section V-B and Section V-C present the landing experiments for a quadrotor and a fixed-wing aircraft, respectively.

A. Tracking Algorithms Experiments

We test our system in five scenes: Scene I was selected to landing the quadrotor under a cloudy weather condition. This scene was selected to evaluate the algorithm's ability to manage the disturbance from cloud, which is usually a challenge mainly for infrared feature recognition. With regard to infrared feature varying due to distinct temperature, two experiments were carried out individually in a high temperature environment (Scene III) and a normal one (Scene IV). In addition, one trial was conducted in Scene IV, a foggy day in the morning, where the stereo system was fixed near the Huanghua airport, Changsha, China. At last, Scene V elaborated that a fixed-wing landing on a simulated carrier deck, more information will be detailed in Section V-C.

The parameters in different algorithms have been tuned manually. For real flying testing (such as in Section V-B and Section V-C), the parameters were selected referenced to laboratory experiments, and if necessary, changing at the flying site. The results of Meanshift, Snakes, Level Set, DRLSE, and Fast Marching are indicated by red, green, blue, pink and yellow contours in Fig. 8 and each column presented one scene. Three typical frames of each scene have been selected to show the accuracy of the five different algorithms. The successful catching percentage in each scene is shown in Table II.

Meanshift can detect the target within clear background such as in Scene II, III and IV in a low percentage. However,

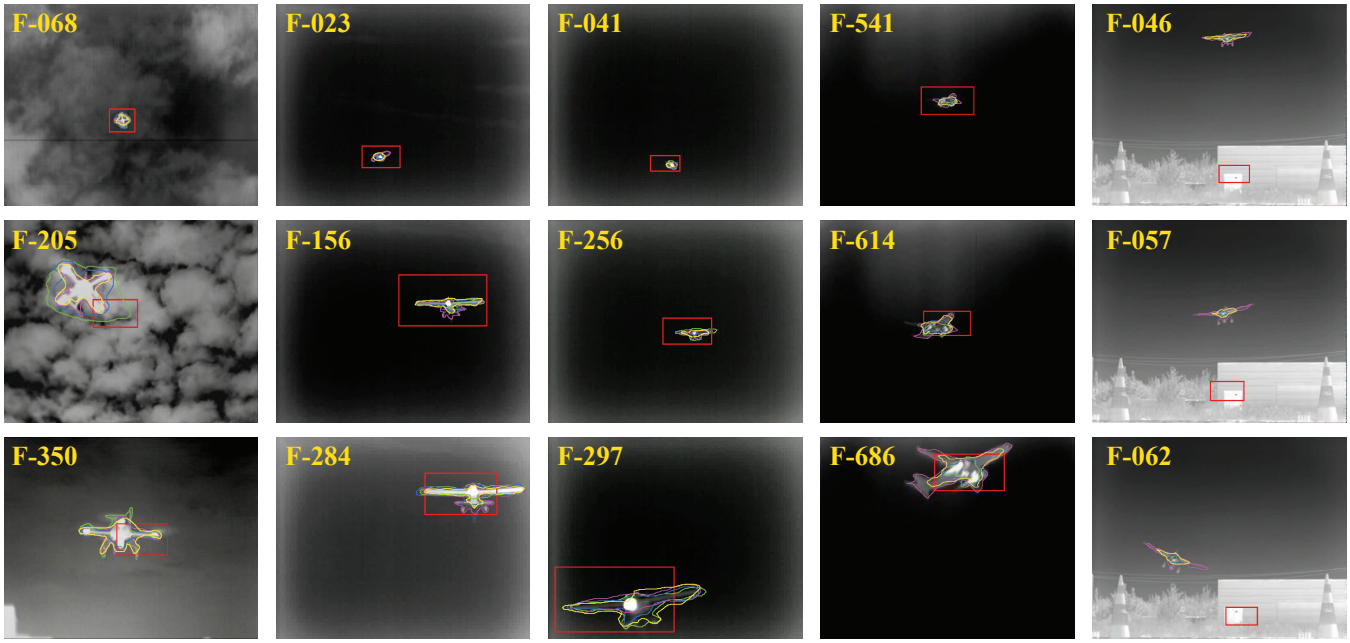

Fig. 8. The typical results of Meanshift, Snakes, Level Set Method, DRLSE, Fast Marching Method are indicated by red, green, blue, pink and yellow contours.

it failed when various clouds in the air (Frame 205 in Scene I) or buildings have similar infrared feature histogram (Frame 046, 057 and 062 in Scene I). Snakes and Level Set Method achieved better results compared to Meanshift, especially in Scene II, III and V. Yet, they also have low performance regarding to manage the disturbance of clouds (Frame 205 in Scene I). For target with complexity features (Frame 614 and 686 in Scene IV), Snakes and Level Set Method cannot catch the center of the target continuously, though only with high detecting percentage. Considering the accurateness of the final contour, DRLSE delicately depicted the edge of aircraft, no matter the target was far away (Frame 156 and 284 in Scene II) or just around the corner (Frame 297 in Scene III). In Scene II, under the high temperature environment, several miniature details were cached such in frame 284 in Scene II, both the landing gear and hook were strictly segmented from the background. However, the drawback of DRLSE is time consuming which is hardly to be used at real-time. More detailed time consuming analyses reference to [48]. Similarly, the Fast Marching Method also successfully caught the target in all five distinctive scenes. Though not all the features were correctly measured, Fast Marching Method indicated a contented cost of timing. The real time operating ability was also demonstrated in [46]. Therefore, given its efficiency and accuracy, Fast Marching Method is the proper algorithm for the stereo vision system.

B. *Quadrotor Aircraft Landing*

We have carried out field experiments during during both day night with similar weather condition (wind speed less than 4 m/s). The procedure of the experiment has been divided into two phases: (1) manually fly the quadrotor into 100 m height but out of the FOV (2) initial and activate the

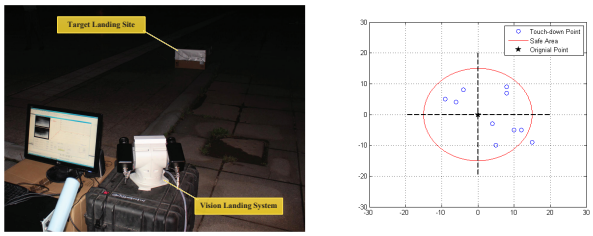

(a) (b)

Fig. 9. (a) Quadrotor down-toch point results. (b) Evening landing system setup.

stereo vision system. When the tracking algorithms detect quadrotor successfully, the flight model will is changed from manually to autonomous. The ideal landing area was set 15 m in front of the landing system. A picture of the system configuration is shown in Fig.9(a), which was taken during a night flight. The center of the ideal landing point was set to (0, 0). The safe area was defined as a disc with 15 cm radius. Table III shows the statistical result of touch-down point which is also visualized in Fig.9(b). The above results demonstrated that the stereo vision systems can successfully guide the quadrotor with a proper precision. The average error in x-axis is 8.1 cm and in y-axis is 6.5 cm. The maximum error and the standard deviation of the flight accuracy show uncritical oscillation around the idea landing point, considering the size of quadrotor(54 cm).

C. *Fixed-wing Aircraft Landing*

For fixed-wing landing, the process can be divided into five segmentations: (1) Catching the aircraft by the vision system; (2) Starting the autonomous landing process. (3) Check the relative position and velocity of the aircraft (if

TABLE III

THE RESULTS OF TOUCH-DOWN POINT ERROR IN TEN EXPERIMENTS

no.	1	2	3	4	5	6	7	8	9	10	m	δ
x	10	8	-6	5	-4	15	-9	8	4	12	8.1	3.57
x	-5	9	4	10	8	-9	5	7	-3	-5	6.5	2.41

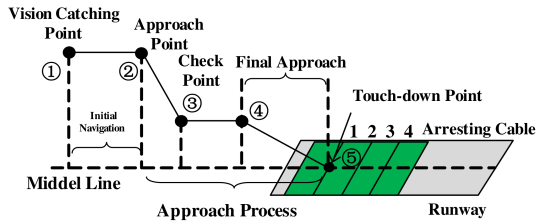

Fig. 10. Fixed-wing landing process.

Fig. 11. Simulated Carrier Deck.

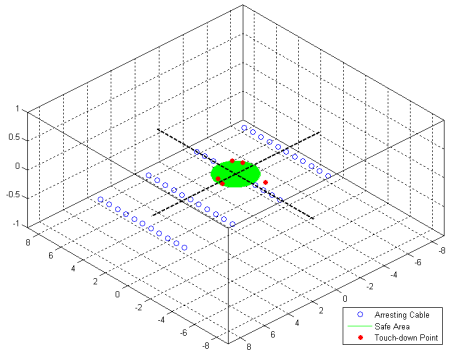

Fig. 12. The result of fixed-wing touch-down point.

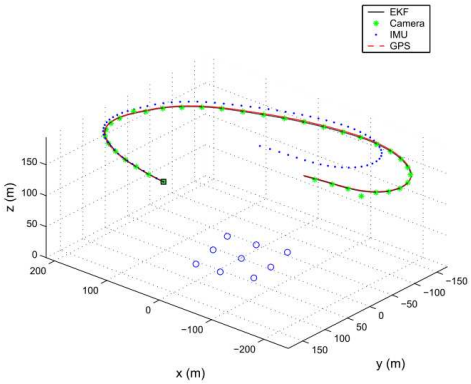

Fig. 13. The position comparation of GPS, IMU, EKT and camera.

not satisfied the safe landing threshold, transfer to missed approach maneuver). (4) Final approach process. (5) Land on ground or hook the arresting cable. The whohe process was shown in Fig.10. Several experiments have been carried out with the fixed-wing aircraft. In December 2011, we counted our system in 1st International UAV Innovation Grand Prix, where a simulated carrier deck was constructed and the landing field consists of a take-off runway, a flying zone, a drop zone and a landing area. The landing runway has a length of 60 m and width of 8 m. In the landing zone, there are four arresting cables which are 4 m away from each other. The cables were set to 30 mm above the landing ground. The goal was to land the UAV autonomously and hook the second arresting cable. The landing area is shown in Fig.11. We set the standard landing point, the middle point of the second arresting cable, to (0, 0). Left deviation and forward deviation were set to positive. Besides, the relation between the safe area (a circle area of 1.5 m radius) and the five touch-down points is depicted in Fig.12. The safe area is shown in green and the arresting cables in blue. Only the fourth touch-down point was out of the general safe circle. In addition, for comparison, the data from GPS, IMU and Vision system have been recorded. The date from one flight is shown in Fig.13. Although the aircraft has not hooked the second arresting cable every time, the autonomous landings were all successful and the error is bounded to less than 2 m. Some videos with eliminated drift demonstrating the robustness of our approach are publicly available: http://tams-www.informatik.uni-hamburg.de/videos/index.php.

VI. CONCLUSIONS

In this research, we presented a novel infrared stereo vision system for UAV autonomous landing in GPS-denied field. Using infrared stereo cameras can reduce both the system cost and complexity of the tracking algorithm. Meanwhile, the search FOV is enlarged significantly by a PTU, in order to catch the aircraft as early as possible. The system has been evaluated according to robustness and precision by several field experiments with a quadrotor or a fixed-wing aircraft, both qualitatively and quantitatively. Although promising results have been obtained, there is still some open problems, such as low accuracy of fixed-wing touch-down points. The near future work is to improve the tracking algorithms and 3D position estimation methods. Besides, to attain higher aircraft status, visual navigation knowledge from the ground station should be properly fused with GPS and IMU.

REFERENCES

[1] F. Kendoul, “Survey of advances in guidance, navigation, and control of unmanned rotorcraft systems,” *Journal of Field Robotics*, vol. 29, no. 2, pp. 315–378, Mar 2012.

[2] J. Wu, Q. Li, M. He, and F. Zhang, *A Terrain Model Generation Method Based on 2D Plan Laser Scanner for Micro UAV Autonomous Flight*. Springer-Verlag, Nov 2013.

[3] J. Vasconcelos, C. Silvestre, P. Oliveira, and B. Guerreiro, "Embedded UAV model and laser aiding techniques for inertial navigation systems," *Control Engineering Practice*, vol. 18, no. 3, pp. 262–278, Mar 2010.

[4] A. Wu and E. Johnson, *Autonomous Flight in GPS-Denied Environments Using Monocular Vision and Inertial Sensors*. American Institute of Aeronautics and Astronautics, Apr 2010.

[5] S. Weiss, D. Scaramuzza, and R. Siegwart, "Monocular-SLAM-based navigation for autonomous micro helicopters in GPS-denied environments," *Journal of Field Robotics*, vol. 28, no. 6, pp. 854–874, Nov 2011.

[6] S. Lange, N. Sünderhauf, P. Neubert, and P. Drews, Sebastianand Protzel, *Autonomous Corridor Flight of a UAV Using a Low-Cost and Light-Weight RGB-D Camera*. Springer-Verlag, 2012.

[7] A. Bachrach, S. Prentice, R. He, P. Henry, A. S. Huang, M. Krainin, D. Maturana, D. Fox, and N. Roy, "Estimation, planning, and mapping for autonomous flight using an rgb-d camera in GPS-denied environments," *The International Journal of Robotics Research*, vol. 31, no. 11, pp. 1320–1343, Sep 2012.

[8] T. Templeton, D. H. Shim, C. Geyer, and S. S. Sastry, *Autonomous Vision-based Landing and Terrain Mapping Using an MPC-controlled Unmanned Rotorcraft*. Institute of Electrical and Electronics Engineers, Apr 2007, pp. 1349–1356.

[9] D. Pebrianti, F. Kendoul, S. Azrad, W. Wang, and K. Nonami, "Autonomous hovering and landing of a quad-rotor micro aerial vehicle by means of on ground stereo vision system," *Journal of System Design and Dynamics*, vol. 4, no. 2, pp. 269–284, 2010.

[10] P. Abbeel, A. Coates, and A. Y. Ng, "Autonomous helicopter aerobatics through apprenticeship learning," *The International Journal of Robotics Research*, vol. 29, no. 13, pp. 1608–1639, Nov 2010.

[11] W. Wang, G. Song, K. Nonami, M. Hirata, and O. Miyazawa, *Autonomous Control for Micro-Flying Robot and Small Wireless Helicopter X.R.B*. Institute of Electrical and Electronics Engineers, Oct 2006, pp. 2906–2911.

[12] Sierra Nevada Corporation, "Tactical automatic landing system." [Online]. Available: http://www.sncorp.com/

[13] J. Farrell, M. Barth, R. Galijan, and J. Sinko, "GPS/INS based lateral and longitudinal control demonstration: Final report," Institute of Transportation Studies, UC Berkeley, Tech. Rep., 1998.

[14] C. Martinez, I. F. Mondragn, M. A. Olivares-Mndez, and P. Campoy, "On-board and ground visual pose estimation techniques for UAV control," *Journal of Intelligent & Robotic Systems*, vol. 61, no. 1-4, pp. 301–320, Jan 2011.

[15] C. Martinez, P. Campoy, I. Mondragon, and M. A. Olivares-Mendez, *Trinocular ground system to control UAVs*. Institute of Electrical and Electronics Engineers, Oct 2009, pp. 3361–3367.

[16] O. Shakernia, Y. Ma, T. J. Koo, and S. Sastry, "Landing an unmanned air vehicle: Vision based motion estimation and nonlinear control," *Asian Journal of Control*, vol. 1, no. 3, pp. 128–145, Sep 1999.

[17] A. Cesetti, E. Frontoni, A. Mancini, P. Zingaretti, and S. Longhi, "A vision-based guidance system for UAV navigation and safe landing using natural landmarks," *Journal of Intelligent and Robotic Systems*, vol. 57, no. 1-4, pp. 233–257, Jan 2010.

[18] R. W. Madison, G. L. Andrews, P. A. DeBitetto, S. A. Rasmussen, and M. S. Bottkol, "Vision-aided navigation for small uavs in gps-challenged environments," *The Draper Technology Digest*, p. 4, 2008.

[19] A. R. Conway, "Autonomous Control of an Unstable Helicopter Using Carrier Phase GPS Only," Master's thesis, Stanford University, March 1995.

[20] R. He, A. Bachrach, M. Achtelik, A. Geramifard, D. Gurdan, S. Prentice, J. Stumpf, and N. Roy, "On the design and use of a micro air vehicle to track and avoid adversaries," *The International Journal of Robotics Research*, vol. 29, no. 5, pp. 529–546, Apr 2010.

[21] S. Scherer, S. Singh, L. Chamberlain, and M. Elgersma, "Flying fast and low among obstacles: Methodology and experiments," *The International Journal of Robotics Research*, vol. 27, no. 5, pp. 549–574, May 2008.

[22] M. C. Bosse, "A vision augmented navigation system for an autonomous helicopter," Ph.D. dissertation, Citeseer, 1997.

[23] O. Amidi, T. Kanade, and K. Fujita, "A visual odometer for autonomous helicopter flight," *Robotics and Autonomous Systems*, vol. 28, no. 2-3, pp. 185–193, Aug 1999.

[24] A. Matsue, W. Hirosue, H. Tokutake, S. Sunada, and A. Ohkura, "Navigation of small and lightweight helicopter," *Transactions of the Japan Society for Aeronautical and Space Science*, vol. 48, no. 161, pp. 177–179, 2005.

[25] S. Bouabdallah, P. Murrieri, and R. Siegwart, "Towards autonomous indoor micro vtol," *Autonomous Robots*, vol. 18, no. 2, pp. 171–183, Mar 2005.

[26] S. Saripalli, J. Roberts, P. Corke, G. Buskey, and G. Sukhatme, *A tale of two helicopters*. Institute of Electrical and Electronics Engineers, 2003, pp. 805–810.

[27] G. Buskey, J. Roberts, P. Corke, and G. Wyeth, "Helicopter automation a using a low-cost sensing system," *Computing Control Engineering Journal*, vol. 15, no. 2, pp. 8–9, 2004.

[28] S. Saripalli, J. Montgomery, and G. Sukhatme, "Visually guided landing of an unmanned aerial vehicle," *IEEE Transactions on Robotics and Automation*, vol. 19, no. 3, pp. 371–380, Jun 2003.

[29] O. Yakimenko, I. Kaminer, W. Lentz, and P. Ghyzel, "Unmanned aircraft navigation for shipboard landing using infrared vision," *IEEE Transactions on Aerospace and Electronic Systems*, vol. 38, no. 4, pp. 1181–1200, Oct 2002.

[30] K. E. Wenzel, P. Rosset, and A. Zell, "Low-cost visual tracking of a landing place and hovering flight control with a microcontroller," *Journal of Intelligent and Robotic Systems*, vol. 57, no. 1-4, pp. 297–311, Jan 2010.

[31] S. Hutchinson, G. Hager, and P. Corke, "A tutorial on visual servo control," *IEEE Transactions on Robotics and Automation*, vol. 12, no. 5, pp. 651 –670, oct 1996.

[32] Y. Zhao and H. Pei, "An improved vision-based algorithm for unmanned aerial vehicles autonomous landing," *Physics Procedia*, vol. 33, pp. 935–941, Jan 2012.

[33] A. Johnson, J. Montgomery, and L. Matthies, *Vision Guided Landing of an Autonomous Helicopter in Hazardous Terrain*. Institute of Electrical and Electronics Engineers, 2005, pp. 3966–3971.

[34] O. Bourquardez and F. Chaumette, *Visual servoing of an airplane for auto-landing*. Institute of Electrical and Electronics Engineers, Oct 2007, pp. 1314–1319.

[35] S. Zingg, D. Scaramuzza, S. Weiss, and R. Siegwart, *MAV navigation through indoor corridors using optical flow*. Institute of Electrical and Electronics Engineers, May 2010, pp. 3361–3368.

[36] J. Engel, J. Sturm, and D. Cremers, "Camera-based navigation of a low-cost quadrocopter," *IMU*, vol. 320, p. 240, 2012.

[37] E. Altug, "Control of a quadrotor helicopter using dual camera visual feedback," *The International Journal of Robotics Research*, vol. 24, no. 5, pp. 329–341, May 2005.

[38] D. Comaniciu and P. Meer, "Mean shift: A robust approach toward feature space analysis," *Pattern Analysis and Machine Intelligence, IEEE Transactions on*, vol. 24, no. 5, pp. 603–619, 2002.

[39] A. Betser, P. Vela, and A. Tannenbaum, "Automatic tracking of flying vehicles using geodesic snakes and kalman filtering," in *Decision and Control, 2004. CDC. 43rd IEEE Conference on*, vol. 2. IEEE, 2004, pp. 1649–1654.

[40] R. J. Sattigeri, E. N. Johnson, A. J. Calise, and J.-C. Ha, "Vision-based target tracking with adaptive target state estimator," 2007.

[41] A. Blake, M. Isard, *et al.*, *Active contours*. Springer London, 1998, vol. 1.

[42] R. Malladi, J. Sethian, and B. Vemuri, "Shape modeling with front propagation: a level set approach," *Pattern Analysis and Machine Intelligence, IEEE Transactions on*, vol. 17, no. 2, pp. 158–175, 1995.

[43] V. Caselles, F. Catte, T. Coll, and F. Dibos, "A geometric model for active contours in image processing," *Numerische Mathematik*, vol. 66, no. 1, pp. 1–31, Dec 1993.

[44] J. A. Sethian, "Curvature and the evolution of fronts," *Communications in Mathematical Physics*, vol. 101, no. 4, pp. 487–499, 1985.

[45] S. Osher and J. A. Sethian, "Fronts propagating with curvature-dependent speed: algorithms based on hamilton-jacobi formulations," *Journal of computational physics*, vol. 79, no. 1, pp. 12–49, 1988.

[46] E. N. Johnson, A. J. Calise, Y. Watanabe, J.-C. Ha, and J. C. Neidhoefer, "Real-time vision-based relative aircraft navigation," 2007.

[47] C. Li, C. Xu, C. Gui, and M. D. Fox, "Distance regularized level set evolution and its application to image segmentation," *IEEE Transactions on Image Processing*, vol. 19, no. 12, pp. 3243–3254, Dec 2010.

[48] C. Li, C. Xu, C. Gui, and M. Fox, *Level Set Evolution without Re-Initialization: A New Variational Formulation*. Institute of Electrical and Electronics Engineers, 2005, pp. 430–436.